

## OCEANOGRAPHY

# Eddy-driven subduction exports particulate organic carbon from the spring bloom

Melissa M. Omand,<sup>1\*</sup> Eric A. D'Asaro,<sup>2</sup> Craig M. Lee,<sup>2</sup> Mary Jane Perry,<sup>3</sup> Nathan Briggs,<sup>3</sup> Ivona Cetinić,<sup>3</sup> Amala Mahadevan<sup>1†</sup>

The export of particulate organic carbon (POC) from the surface ocean to depth is traditionally ascribed to sinking. Here, we show that a dynamic eddying flow field subducts surface water with high concentrations of nonsinking POC. Autonomous observations made by gliders during the North Atlantic spring bloom reveal anomalous features at depths of 100 to 350 meters with elevated POC, chlorophyll, oxygen, and temperature-salinity characteristics of surface water. High-resolution modeling reveals that during the spring transition, intrusions of POC-rich surface water descend as coherent, 1- to 10-kilometer-scale filamentous features, often along the perimeter of eddies. Such a submesoscale eddy-driven flux of POC is unresolved in global carbon cycle models but can contribute as much as half of the total springtime export of POC from the highly productive subpolar oceans.

The biological carbon pump (1), coupled with physical processes, makes the North Atlantic ocean a perennial and substantial sink of atmospheric CO<sub>2</sub> (2, 3). Seasonally, strong winter-time cooling and winds enhance CO<sub>2</sub> solubility (4) and gas transfer, drive convective and turbulent circulations deepening the mixed layer, sequester carbon (5), and entrain nutrients into the mixed layer. With the onset of spring, increasing light, a shoaling mixed layer (6), enhanced stratification (7), and suppressed turbulent convection (8) lead to exceptionally high rates of phytoplankton production, resulting in a bloom. A critical piece of the carbon cycle is the ensuing export of organic carbon from the surface productive layer to the mesopelagic (100 to 1000 m). Traditionally, carbon-flux studies in the region have focused on export by sinking particles (9). Models have been used to infer the contribution of oceanic subduction to carbon export, most often described in terms of large-scale water-mass transformation and advection over seasonal time scales (10–12). Here, using observations complemented by a high-resolution physical-biological process model, we present evidence that export also occurs through localized subduction of small, nonsinking particulate carbon (Fig. 1A). The intensification of fronts within the eddying flow field, through convergence, frontogenesis, and wind-forcing, generates downward velocities (13, 14) along sloping isopycnal surfaces that create subsurface intrusions of the surface water (15, 16). The resulting eddy-driven sub-

duction at scales of order 1 to 10 km leads to episodic injections of water from the surface mixed layer (17, 18) (Fig. 1A) and net transport of particulate organic carbon (POC) to depth (19, 20).

During the North Atlantic Bloom study of 2008 (NAB08), we carried out intensive observations of the onset (7) and progression of the spring bloom. The observations were made within the water-following reference frame provided by a Lagrangian mixed-layer float, sampled spatially by four autonomous Seaglider robots at distances of 1 to 50 km from the float. The gliders measured chlorophyll fluorescence (Chl F), optical backscatter (a proxy for POC), oxygen, salinity, temperature, and pressure. Analysis was performed on 774 glider profiles (to 1000 m) obtained over 25 days starting (at yearday 120; yearday 1 is 1 January 2008) a few days after the onset of the bloom. The backscatter and Chl F records were filtered to remove spikes caused by large, sinking aggregates (21), likely containing diatom spores (22), and the remaining signal was attributed to small POC with negligible sinking rates. The co-occurrence of POC and Chl F in ratios typical of phytoplankton suggests that a good fraction of these particulates were live phytoplankton cells.

In 9.2% of the analyzed glider profiles, we observed distinct subsurface maxima [see the supplementary materials, section S1.3 (SM S1.3)] in POC, Chl F, and oxygen co-occurring with anomalous temperature-salinity properties (“spice”) (fig. S2) characteristic of the surface mixed layer (Fig. 1, B and C). These lateral intrusions of water (27) extending downward from the surface occurred at depths ranging from 100 to 350 m, well below the mixed layer and euphotic zone where phytoplankton can grow. In fact, 63 (of 71) subsurface maxima in POC collapse onto distinct potential density surfaces (isopycnals), suggesting that these are multiple observations of the

same few intruding features (Fig. 1D). The dynamic height estimated from an objective map of glider-based depth-averaged currents (SM S1.2) from this period indicates that the platforms (float and gliders) were orbiting an anticyclonic eddy (Fig. 1E). Theory and modeling suggest that such regions of enhanced vorticity are preferred locations for subduction (15).

The subsurface intrusion of surface water with elevated POC in the density range  $\sigma_t = 27.43 \pm 0.01 \text{ kg m}^{-3}$  (purple segments, Fig. 1, C and D) was sampled multiple times over a span of 17 days (yeardays 128 to 145) (Fig. 1E). The data suggest that this isopycnal was in the mixed layer before yearday 130, after which it remained below the mixed layer and euphotic zone, isolated from light or air-sea gas exchange for at least 17 days, which is sufficiently long for remineralization to return the organic material to dissolved inorganic form. As the bloom developed, POC increased and oxygen became increasingly supersaturated in the surface mixed layer. The apparent oxygen utilization (AOU) calculated with reference to saturation at the surface was thereby negative (open circles, Fig. 2) in the mixed layer. Within the subsurface features, the oxygen and POC decreased (filled circles, Fig. 2) and AOU became positive. We interpret the increase in mixed-layer POC and oxygen as resulting from photosynthesis, and their subsurface depletion as resulting from respiration of organic carbon. The ratio between changes in the AOU (or oxygen) and POC is  $\sim 1.5$  (Fig. 2), a respiratory quotient consistent with previous observations (23). Assuming negligible ventilation or photosynthesis, the rates of oxygen utilization imply a remineralization rate of  $0.4 \text{ mmol O}_2 \text{ m}^{-3} \text{ d}^{-1}$  between yeardays 130 and 145, consistent with previous estimates in the North Atlantic (24).

Eddy-driven subduction was mechanistically explored with a three-dimensional process-study ocean model (25) coupled to a simple phytoplankton model with a light-dependent growth rate (26) (SM S2). The domain is 480 km in meridional extent and 96 km east-west, with periodic boundaries in the zonal direction. The model is initialized in midwinter (yearday 30), with three fronts spanning the domain; forced with winds; and allowed to evolve for 4 months (7). By yearday 120 (the start of the observations presented here), the modeled phytoplankton bloom is well developed. The light-dependent growth of phytoplankton results in high concentrations of POC near the surface, particularly where stratification has set in. The model shows eddies with filaments of positive and negative vorticity (Fig. 3A) that correspond with horizontal gradients in buoyancy and enhanced POC (Fig. 3B). Downward-sloping, tongue-like intrusions of water rich in POC extend from the surface into the interior. Vertical profiles through these features (Fig. 3C) are remarkably similar to the glider profiles. Approximately 10% of the model profiles exhibit subsurface maxima, similar in prevalence to the observations. Projected onto a horizontal surface at 200 m, profiles with

<sup>1</sup>Woods Hole Oceanographic Institution, Woods Hole, MA 02543, USA. <sup>2</sup>Applied Ocean Physics Laboratory, University of Washington, Seattle, WA 98195, USA. <sup>3</sup>Darling Marine Center, University of Maine, Walpole, ME 04573, USA.

\*Present address: Graduate School of Oceanography, University of Rhode Island, Narragansett, RI 02882, USA. †Corresponding author. E-mail: amala@whoi.edu

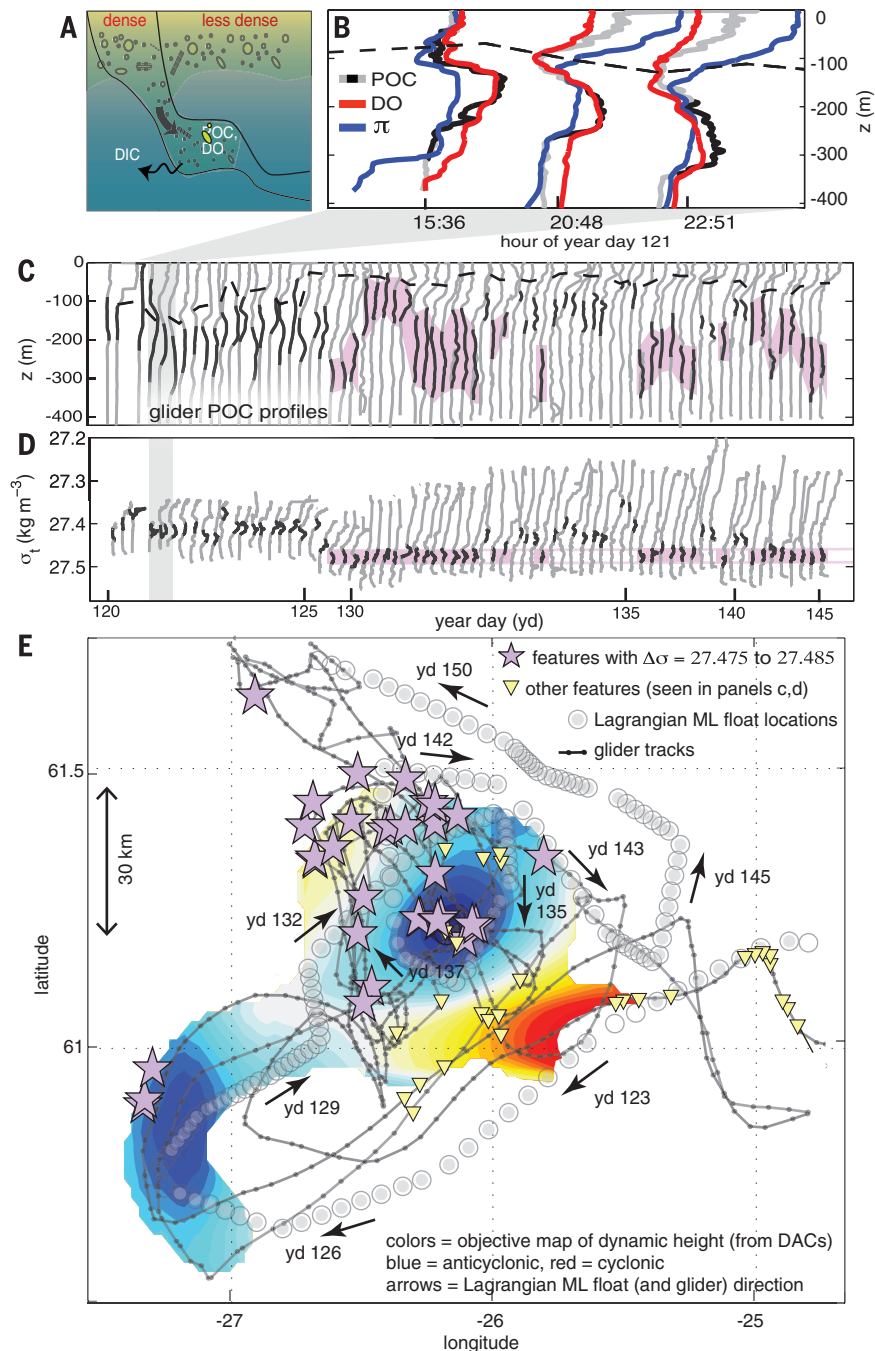


**Fig. 1. (A)** Eddy-driven subduction transports POC- and oxygen-rich surface water along tilted isopycnals. **(B)** Examples of Seaglider profiles of POC (gray, range  $71 \text{ mg m}^{-3}$ ), dissolved oxygen (DO) (red, range  $25 \text{ mmol m}^{-3}$ ), and spice ( $\pi$ , blue, range  $0.17 \text{ kg m}^{-3}$ ) from yearday 121 show features with elevated concentrations below the mixed layer (depth defined by  $\Delta\sigma_t = 0.03$ , dashed black line). **(C)** Thirty-day time series of 71 (of 772) POC profiles with distinct subsurface features versus depth. Black segments indicate the  $\sigma_t$  span ( $0.005$ ) of each feature. **(D)** POC profiles from (C) versus  $\sigma_t$ , with 33 of the features falling within the same water mass (defined by  $\sigma_t = 27.48 \pm 0.005 \text{ kg m}^{-3}$ ) indicated by purple shading. **(E)** Locations of the subsurface features (colored symbols) from (C) and (D) overlaid on the tracks of the Seagliders (gray lines) and mixed-layer float (open circles, locations shown every 3 hours). The approximate location and yearday of the mixed-layer float is indicated by arrows. Most features were observed in the vicinity of anticyclonic regions (the dynamic height is shown in colors, with anticyclonic streamlines indicated by blue colors and an overall range of  $8 \text{ cm}$ ), based on objective mapping of the depth-averaged currents (DAC) from gliders.

deep local maxima in POC are clustered in coherent streaks and patches, most often in regions of subsurface negative vorticity (black points, Fig. 3, A and B). The probability distributions of depth-averaged currents, POC concentration, isopycnal depth, and isopycnal tilts are very similar in the model and observations (SM S2.1), giving us confidence that the model captures the temporal and spatial scales of both the physics and biology and can thus be used to estimate the POC flux due to eddy-driven subduction.

The intensification of fronts on the peripheries of mixed-layer eddies drives secondary ageostrophic circulations, generating vertical velocities of approximately  $30 \text{ m d}^{-1}$  and ageostrophic cross-front flows of  $3$  to  $5 \text{ cm s}^{-1}$  (15). This ageostrophic flow is largely along isopycnal surfaces and carries water from the surface layer, below and across the front, and delivers its contents to the stratifying interior (19). Similarly, the secondary circulations transport water from the base of the mixed layer to the surface. Because POC is produced in the sunlit surface layers as the mixed layer is stratifying, there is a strong vertical gradient in POC. This results in a net downward flux of POC.

The vertical flux of POC in the model is the covariance between POC anomalies, defined as  $c' = \text{POC} - \langle \text{POC} \rangle$ , and vertical velocity  $w'$ , calculated as  $\text{Flux} = \langle w'c' \rangle$ , where angle brackets denote the horizontal average at each depth (shown at  $100 \text{ m}$  in Fig. 4A). On average, a negative covariance (subduction of POC) results from downward transport of POC-rich water

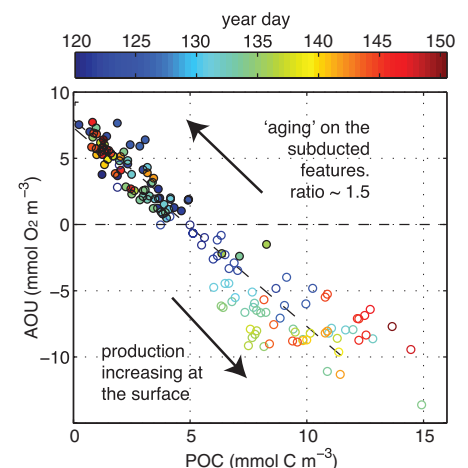
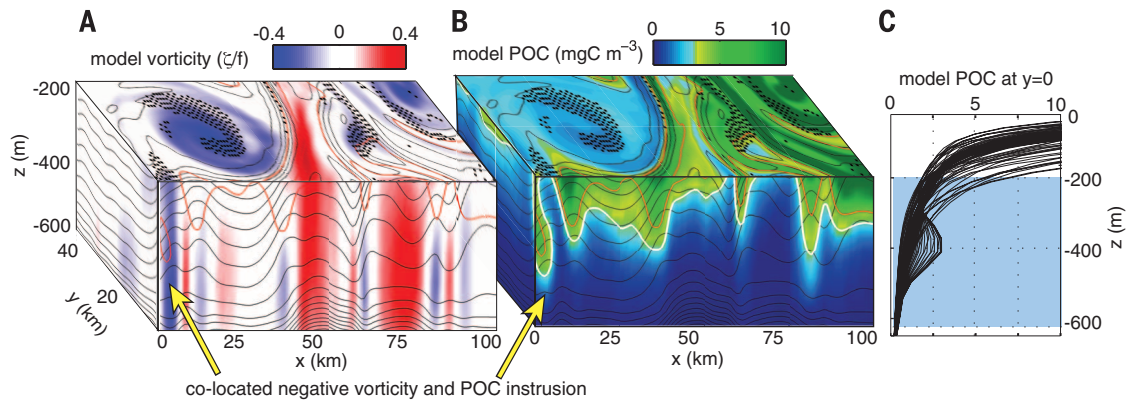


**Fig. 2.** AOU versus POC averaged within the subducted features (solid circles) and over the mixed layer (open circles), colored by yearday. The AOU increases as the POC decreases on the subducted features over time, indicative of respiration and diverging from simultaneously measured surface values. The best fit to the filled circles (dashed black line) has a slope of  $1.5$ , consistent with a respiratory quotient arising from bacterial metabolism. AOU is defined as the difference between the saturation oxygen (at measured temperature, salinity, and surface pressure) and the measured oxygen.

**Fig. 3. A subdomain of modeled (A) relative vorticity ( $\zeta$ ) normalized by planetary vorticity ( $f$ ) and (B) POC from 200 to 600 m depth on yearday 125.** The  $x$ - $y$  locations of subsurface features identified with the model are indicated by black points in the  $z = 200$  m plane. Black lines indicate the potential density ( $\sigma_t$ ) contours. The domain is selected to intersect a region at the periphery of an anti-cyclone, containing high



POC and deep negative vorticity consistent with frontogenetic subduction. (C) Examples of 96 model POC ( $\text{mgC m}^{-3}$ ) profiles at  $y = 0$  show that roughly 10% contain subsurface features of elevated POC similar to the observations with Seagliders. The depth range shown in (A) and (B) is indicated by blue shading.

and upward transport of water relatively devoid of POC. Our model shows that  $w'$ ,  $c'$ , and their covariance are coherent in filaments that are just a few kilometers in width (fig. S10) and deliver water to depths approaching the winter mixed layer. Model diagnostics suggest that only a small fraction of the subducted water is re-entrained into the mixed layer, and this occurs mostly within the first 2 days. More than 75% of the water remains subducted until the end of the model simulation (a further 10 days), suggesting that it would remain below the mixed layer over the course of the summer (SM S2.2).

We parameterize the eddy-driven flux of POC  $\langle w'c' \rangle$  in terms of the eddy-driven vertical flux of buoyancy  $\langle w'b' \rangle = \psi_e M^2$  (28), where  $\psi_e$  is the overturning stream function arising from mixed-layer eddies and  $M^2 = |\nabla_H b|$  is the characteristic horizontal gradient of buoyancy  $b = -g\rho_0^{-1}(\rho - \rho_0)$  in the mixed layer. We use an existing parameterization,  $\psi_e \sim C_e M^2 H^2 f^{-1}$  (29), where  $H$  is the mixed layer depth,  $f$  is the Coriolis parameter, and  $C_e = 0.08$  is a scaling constant. The vertical POC flux must account for the fact that isosurfaces of POC are not aligned with the isopycnal surfaces (isosurfaces of  $b$ ). Whereas the isopycnals are sloping, the POC gradient is largely vertical. Thus,  $\langle w'c' \rangle \sim \langle w'b' \rangle \langle \frac{\partial \text{POC}}{\partial z} \rangle \langle b_z \rangle^{-1}$ . We evaluate  $\langle \frac{\partial \text{POC}}{\partial z} \rangle$  as  $[\text{POC}]/H^*$ , where  $[\text{POC}]$  is the spatial average of surface POC, and  $H^*$  is the depth of the photosynthetically productive surface layer taken to be  $H$  in the North Atlantic but set equal to the euphotic layer when it is deeper than  $H$  (SM S3.4.1). The resulting scaling estimate for the vertical flux of POC due to eddy-driven subduction (see SM S3.3 for details) is therefore

$$\text{Flux} = \langle w'c' \rangle \sim \psi_e \Gamma [\text{POC}]/H^* \quad (1)$$

where  $\Gamma = M^2/\Lambda^2 = |\nabla b|/b_z$  represents the mean slope of the isopycnals in the restratifying region.

Spatially integrated, the export of POC by eddy-driven subduction is time dependent and varies with mixed-layer depth, vertical and lateral buoyancy gradients, and the surface concentration of POC. Using domain-averaged values of  $M^2$ ,  $N^2$ ,  $H$ , and surface POC over the upper

50 m of our model, we find that our scaling estimate (Eq. 1) captures the mean (Fig. 4A) and 88% of the variability in the domain-averaged flux at 100-m depth, calculated directly from the model as  $F_{100} = \langle w'c' \rangle$  (fig. S14, B and C). The maximal flux occurs when the mixed layer is stratifying but is still deep in places, stratification is patchy, lateral buoyancy gradients exist, and the bloom has begun—i.e.,  $[\text{POC}]$  is high. In our model, we observe that the POC flux  $F_{100}$  increases from yearday 120 as the upper ocean becomes stratified and the bloom grows (Fig. 4A), attaining values of  $170 \text{ mgC m}^{-2} \text{ d}^{-1}$ . Later, although the near-surface POC continues increasing (fig. S13A), the POC flux due to subduction is restricted to a much shallower region as the mixed layer shoals and stratification intensifies, leading to a reduction in  $F_{100}$  to roughly  $50 \text{ mgC m}^{-2} \text{ d}^{-1}$ . Eddy-induced fluxes act mainly along sloping isopycnal surfaces (30), and eddy-driven subduction of POC is most effective when a phytoplankton bloom occurs in conjunction with eddy-driven stratification (7).

Comparing our estimate of the eddy-driven POC flux with the sinking export of POC is not straightforward, because observations of sinking flux events are usually local and not integrated in space and time. Concurrent estimates from NAB08 based on nitrate, POC, and dissolved oxygen indicated that the total carbon export peaked at  $984 \text{ mgC m}^{-2} \text{ d}^{-1}$  (23). Export diagnosed from  $^{234}\text{Th}$  disequilibria over a similar period (in May) was up to  $500 \text{ mgC m}^{-2} \text{ d}^{-1}$  (31). During the short-lived diatom bloom observed within a patch of productive water, sinking export of large particulates was estimated as  $514 \text{ mgC m}^{-2} \text{ d}^{-1}$  (21) at a depth of 100 m. During the Joint Global Ocean Flux Study North Atlantic Bloom Experiment campaign, the export flux of sinking particles peaked at  $492 \text{ mgC m}^{-2} \text{ d}^{-1}$  in early May (32). In comparison with event-based estimates of sinking export (21, 32), eddy-driven subduction of POC accounts for about 25% of the total export flux.

To arrive at an integrated estimate of the eddy-driven POC subduction globally in spring, we evaluate our scaling (Eq. 1) with the Sea-

Viewing Wide Field-of-View Sensor (SeaWiFS) satellite-derived surface POC and the Monthly Isopycnal and Mixed-Layer Ocean Climatology, from which we derive mixed-layer depth  $H$ , vertical and lateral buoyancy gradients  $N^2$  and  $M^2$  during March through May for the Northern Hemisphere, and September through November for the Southern Hemisphere, respectively (SM S3.4 and fig. S15). The largest fluxes occur in regions with seasonally varying mixed layers (Fig. 4B). We compare this estimate to the total export, which includes the sinking flux of POC estimated from satellite data with a model (33), and our estimate of eddy-driven subduction. During the spring, our estimate suggests that eddy-driven subduction of POC contributes as much as half the total export of POC in the North Atlantic, the Kuroshio extension, and the Southern Ocean (Fig. 4C). The covariation of high POC, lateral buoyancy gradients, and relatively deep winter mixed layers provides the conditions for mixed-layer eddies, which during the early spring bloom drive a subduction of POC and oxygen, as evidenced from our observations and modeling. Such a mechanism for the export of POC, dissolved organic matter, and oxygen is unresolved in global climate models.

Previous estimates of POC export have typically fallen short of closing the budget for carbon in the mesopelagic ocean (34, 35). Disaggregation of large POC by zooplankton (36) and the de-trainment of POC-rich water from the mixed layer by seasonal stratification via the so-called mixed-layer pump (5) are some of the mechanisms that have been invoked to reconcile this budget and explain the export of small particles (0.2 to 20  $\mu\text{m}$ ) to depths up to 1000 m in the Norwegian Sea (37). The high spatiotemporal resolution of our observations and modeling points, however, to an alternate pathway for carbon export. Unlike the mixed-layer pump, this mechanism transports water from the most productive surface layers as they experience eddy-driven stratification and rapid growth of phytoplankton due to enhanced light exposure. The fate of the subducted carbon, and its potential to be sequestered for long periods, depends

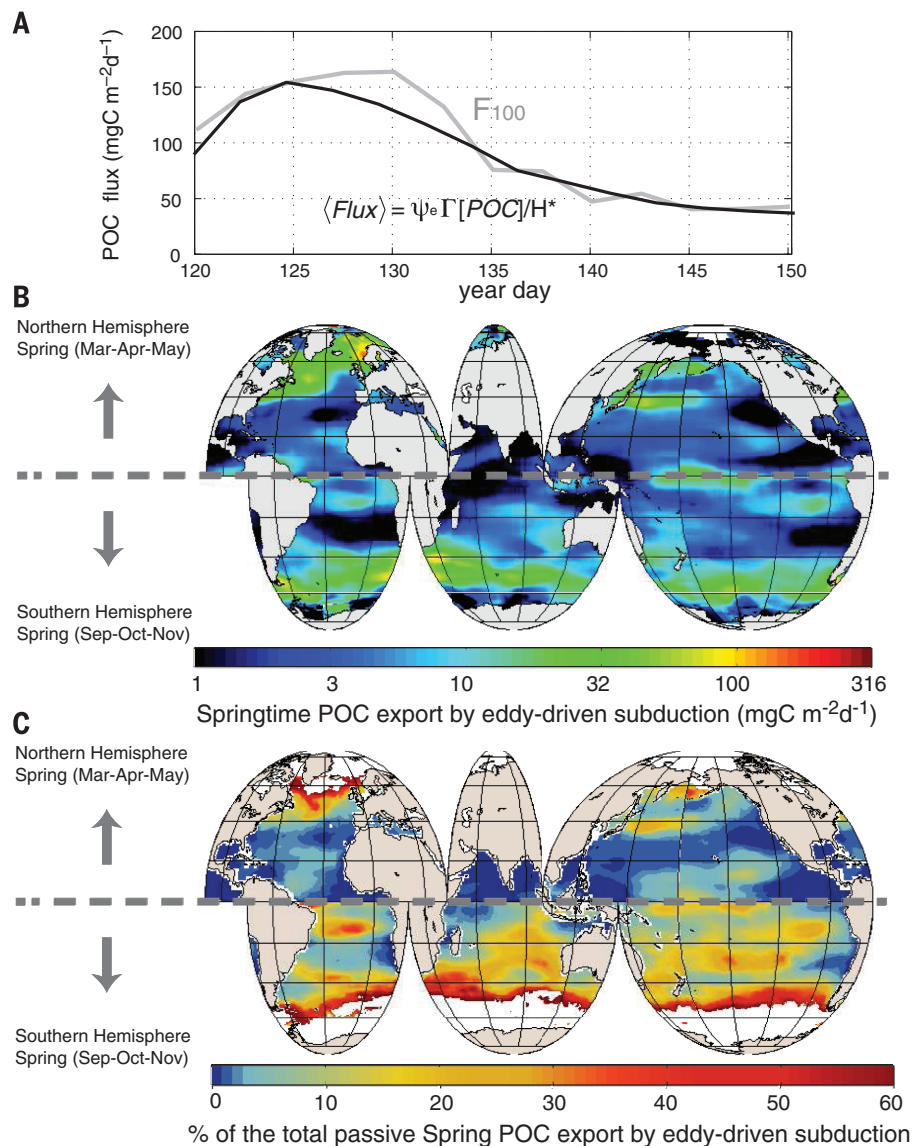


**Fig. 4. Model-based estimate of eddy-driven subduction of POC.** (A) The model-derived flux of POC  $F_{100} = \langle POC \rangle$  at 100-m depth is compared with a model-based scaling estimate  $F_{lux} = \psi_e \Gamma \frac{[POC]}{H^*}$ . The two are correlated with  $r^2 = 0.88$ . (B) A global estimate of eddy-driven subduction of POC. (C) The contribution of eddy-driven subduction [shown in (B)] as a percentage of the total export of POC. The total POC export is defined as the sinking export (33) plus the eddy-driven export (fig. S18).

on several factors, including lateral advection by the large-scale circulation.

In the ocean, large cells and aggregates of organic matter are exported efficiently by sinking. But the total POC biomass is roughly evenly distributed among all size classes due to the relatively large numbers of small cells and particles that constitute a large fraction of the net primary production (38). Eddy-driven subduction provides an export pathway for the small size classes of POC and likely also dissolved organic carbon. (DOC) Such a subduction of small cells substantially augments the POC export arising from the sinking of large particles. Small particles and DOC provide an important source of organic carbon to the microbial food webs (36), and because the sub-

duction is spatially heterogeneous, we anticipate that it stimulates hot spots of microbial activity that have implications for mesopelagic ecology.

#### REFERENCES AND NOTES

1. R. Sanders *et al.*, *Prog. Oceanogr.* **129**, 200–218 (2014).
2. A. Körtzinger *et al.*, *J. Geophys. Res.* **113** (C4), C04020 (2008).
3. C. L. Sabine *et al.*, *Science* **305**, 367–371 (2004).
4. M. J. Follows, R. G. Williams, J. C. Marshall, *J. Mar. Res.* **54**, 605–630 (1996).
5. W. D. Gardner, S. P. Chung, M. J. Richardson, I. D. Walsh, *Deep Sea Res. Part II Top. Stud. Oceanogr.* **42**, 757–775 (1995).
6. H. U. Sverdrup, *J. Cons. Int. Explor. Mer* **18**, 287–295 (1953).

7. A. Mahadevan, E. D'Asaro, C. Lee, M. J. Perry, *Science* **337**, 54–58 (2012).
8. J. Taylor, R. Ferrari, *Limnol. Oceanogr.* **56**, 2293–2307 (2011).
9. H. W. Ducklow, R. P. Harris, *Deep Sea Res. Part II Top. Stud. Oceanogr.* **40**, 1–8 (1993).
10. J. B. Sallée, R. J. Matear, S. R. Rintoul, A. Lenton, *Nat. Geosci.* **5**, 579–584 (2012).
11. J. A. Barth, *J. Geophys. Res.* **107** (C6), 3057 (2002).
12. P. Karleskind, M. Lévy, L. Memery, *J. Geophys. Res.* **116** (C2), C02025 (2011).
13. A. Mahadevan, *Ocean Model.* **14**, 222–240 (2006).
14. A. Mahadevan, A. Tandon, *Ocean Model.* **14**, 241–256 (2006).
15. M. A. Spall, *J. Geophys. Res.* **100** (C2), 2543–2557 (1995).
16. M. Lee, A. Nurser, *J. Phys. Oceanogr.* **42**, 1762–1780 (2012).
17. J. C. McWilliams, F. Colas, M. J. Molemaker, *Geophys. Res. Lett.* **36**, L18602 (2009).
18. M. Lévy, P. Klein, A. M. Treguier, *J. Mar. Res.* **59**, 535–565 (2001).
19. R. Pollard, L. Regier, *Nature* **348**, 227–229 (1990).
20. S. Fielding *et al.*, *J. Mar. Syst.* **30**, 287–304 (2001).
21. N. Briggs *et al.*, *Deep Sea Res. Part I Oceanogr. Res. Pap.* **58**, 1031–1039 (2011).
22. T. Rynearson *et al.*, *Deep Sea Res. Part I Oceanogr. Res. Pap.* **82**, 60–71 (2013).
23. M. B. Alkire *et al.*, *Deep Sea Res. Part I Oceanogr. Res. Pap.* **64**, 157–174 (2012).
24. J. B. Palter, M. S. Lozier, R. T. Barber, *Nature* **437**, 687–692 (2005).
25. A. Mahadevan, J. Olinger, R. Street, *J. Phys. Oceanogr.* **26**, 1868–1880 (1996).
26. W. Bagniewski, K. Fennel, M. J. Perry, E. A. D'Asaro, *Biogeosciences* **8**, 1291–1307 (2011).
27. T. Johnston, O. Cheriton, J. T. Pennington, F. P. Chavez, *Deep Sea Res. Part II Top. Stud. Oceanogr.* **56**, 246–259 (2009).
28. I. Held, T. Schneider, *J. Atmos. Sci.* **56**, 1688–1697 (1999).
29. B. Fox-Kemper, R. Ferrari, R. Hallberg, *J. Phys. Oceanogr.* **38**, 1145–1165 (2008).
30. A. Mahadevan, A. Tandon, R. Ferrari, *J. Geophys. Res.* **115** (C3), C03017 (2010).
31. P. Martin *et al.*, *Deep Sea Res. Part I Oceanogr. Res. Pap.* **58**, 338–349 (2011).
32. K. O. Buesseler, M. P. Bacon, J. K. Cochran, H. D. Livingston, *Deep-Sea Res. A, Oceanogr. Res. Pap.* **39**, 1115–1137 (1992).
33. D. A. Siegel *et al.*, *Global Biogeochem. Cycles* **28**, 181–196 (2014).
34. D. Steinberg *et al.*, *Limnol. Oceanogr.* **53**, 1327–1338 (2008).
35. A. Burd *et al.*, *Deep Sea Res. Part II Top. Stud. Oceanogr.* **57**, 1557–1571 (2010).
36. S. L. Giering *et al.*, *Nature* **507**, 480–483 (2014).
37. G. Dall'Olmo, K. A. Mork, *Geophys. Res. Lett.* **41**, 2921–2927 (2014).
38. T. L. Richardson, G. A. Jackson, *Science* **315**, 838–840 (2007).

#### ACKNOWLEDGMENTS

M.M.O. and A.M. were supported by the National Science Foundation (NSF OCE 1260080, 1434788), the Office of Naval Research, and a fellowship to A.M. from the Radcliffe Institute for Advanced Study. The NAB08 field experiment was supported by NSF OCE-0628107 and OCE-0628379 and NASA NNX-08AL92G. Data from NAB08 is publicly available at the Biological and Chemical Oceanography Data Management Office: <http://osprey.bcodmo.org/project.cfm?flag=view&id=102&sortby=project>.

#### SUPPLEMENTARY MATERIALS

[www.sciencemag.org/content/348/6231/222/suppl/DC1](http://www.sciencemag.org/content/348/6231/222/suppl/DC1)  
Materials and Methods  
Figs. S1 to S18  
Table S1  
References (39–51)

15 August 2014; accepted 4 March 2015  
Published online 26 March 2015;  
10.1126/science.1260062



## Eddy-driven subduction exports particulate organic carbon from the spring bloom

Melissa M. Omand *et al.*

*Science* **348**, 222 (2015);

DOI: 10.1126/science.1260062

*This copy is for your personal, non-commercial use only.*

If you wish to distribute this article to others, you can order high-quality copies for your colleagues, clients, or customers by [clicking here](#).

Permission to republish or repurpose articles or portions of articles can be obtained by following the guidelines [here](#).

**The following resources related to this article are available online at [www.sciencemag.org](http://www.sciencemag.org) (this information is current as of April 9, 2015):**

**Updated information and services**, including high-resolution figures, can be found in the online version of this article at:

<http://www.sciencemag.org/content/348/6231/222.full.html>

**Supporting Online Material** can be found at:

<http://www.sciencemag.org/content/suppl/2015/03/25/science.1260062.DC1.html>

This article **cites 50 articles**, 5 of which can be accessed free:

<http://www.sciencemag.org/content/348/6231/222.full.html#ref-list-1>

This article appears in the following **subject collections**:

Geochemistry, Geophysics

[http://www.sciencemag.org/cgi/collection/geochem\\_phys](http://www.sciencemag.org/cgi/collection/geochem_phys)